TOC Graphic

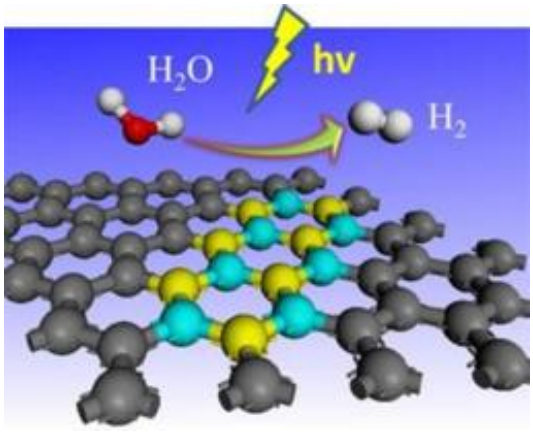

We report here a facile synthesis of graphene decorated with in-plane boron nitride domains (BN-G) and uncover that the formation of BN domains in graphene is critical for engineering the band gap and resulting in an improved activity for photocatalytic hydrogen generation.

Graphene with Atomic-level In-plane Decoration of *h*-BN Domains for Efficient Photocatalysis

Mengzhu Li,[a] Yiou Wang,[b] Pei Tang,[a] Nanhong Xie,[d] Yunxuan Zhao,[c] Xi Liu,[e] Gang Hu,[f] Jinglin Xie,[a] Yufei Zhao,*[c] Junwang Tang,[b] Tierui Zhang,[c] Ding Ma*[a]

[a.] *College of Chemistry and Molecular Engineering, Peking University, Beijing 100871, China.*

[b.] *Department of Chemical Engineering, University College London, London WC1E 7JE, UK.*

[c.] *Key Laboratory of Photochemical Conversion and Optoelectronic Materials, Technical Institute of Physics and Chemistry, Chinese Academy of Sciences, Beijing 100190, China.*

[d.] *Innovative Catalysis Program, Key Laboratory of Organic Optoelectronics & Molecular Engineering, Department of Chemistry, Tsinghua University, Beijing 100084, China.*

[e.] *Syncat@Beijing, Synfuels China Technology Co., Ltd, Beijing 101407, China.*

[f.] *Israel Chemicals Limited, Shanghai 200021, China.*

ABSTRACT: Band gap opening and engineering is one of the tremendous aims in developing novel materials for photocatalytic hydrogen generation. We report here a facile synthesis of graphene decorated with in-plane boron nitride domains by controlling both the doping sequence of heteroatoms and the oxygen content of graphene precursor,

showing significant differences in the doping pattern compared with B and/or N single- or co-doped graphene. We uncover that the formation of BN domains in graphene is critical for engineering the band gap and resulting in an improved activity for photocatalytic hydrogen generation in the absence of any photosensitizer. This work paves the way for the rational design and construction of graphene-based photocatalysts for efficient photocatalysis.

INTRODUCTION

The nanostructured graphene materials have attracted considerable attentions for both fundamental studies and practical applications in the fields of photocatalysis, optoelectronics, lithium batteries, and microelectronics.[1,2] Among them, the seeking of suitable graphene-based photocatalysts for the efficient harvesting and utilization of solar energy is a promising and urgent challenge, as it can alleviate the increasing concerns on fossil fuel depletion and environmental issues.[2] To date, various semiconductor/graphene hybrid catalysts (*e.g.* TiO_2/graphene, WO_3/graphene) have been successfully synthesized and utilized in pollutant degradation, photoreduction of CO_2 and especially, water splitting into hydrogen.[3] In these cases, graphene was generally used as a decent support because of its superior electron mobility, high surface area, and good chemical stability.[1,3] The interface between graphene and semiconductor played an important role in activity enhancement of these catalysts, mainly due to the improved separation efficiency of photoexcited electrons and holes for the electron delocalization effect between semiconductor and graphene.[4-6] Nevertheless, ideal graphene is a two-dimensional (2D) carbon material with no obvious electronic band gap,[4] making it unable to directly absorb the light energy, which restricts its further advances in

photocatalytic applications. Therefore, it is desirable to engineer the band gap of graphene with semiconductive property for the utilization of solar energy.

Recently, diversified methods have been developed to enlarge the band gap and engineer the semiconductive properties of graphene,[7] amongst which, heteroatom doping is considered as a facile and effective strategy.[8,9] Until now, many heteroatoms (*e.g.*, O, N, B, P, I and S) have been successfully doped into graphene,[10,11] for example, doping N or P atoms was revealed to be effective in enhancing the activity of graphene for photocatalytic hydrogen evolution.[12-14] Compared with single element doping strategy, co-doping graphene by two or more kinds of different elements is expected to be more efficient in photocatalytic enhancement of graphene, since it can create a unique electronic structure with a synergistic coupling effect between these heteroatoms.[7] B and N are often the ideal choices for doping of graphene, due to their relative lower (2.04 for B) and higher electronegativity (3.04 for N) than carbon (2.55 for C), respectively.[15] It has also been confirmed that co-doping graphene with B and N atoms was effective for modifying the electronic properties of graphene and even creating new active sites. [16,17] More importantly, recent experimental and theoretical studies on two-dimensional (2D) atomic layered materials have revealed that embedding hexagonal boron nitride domains (*h*-BN) into graphene can produce unique planar heterostructures and tailorable electronic properties.[18,19] For example, the doping of isoelectronic *h*-BN was able to directly open the π–π^* band and tune the band gap of graphene.[7,20-22] However, the conventional strategy for doping graphene with B, N atoms or *h*-BN structures always employed a chemical vapor deposition (CVD) process,[17,18,23] which was costly and difficult for the large-scale preparation and application. Moreover, due to the lack of controllable doping

method, various doping structures (or patterns) involving B, N and graphene would be formed as follows: (1) B and N atoms were homogeneously doped into graphene to form separate B-C and N-C bonds;[15] (2) atomic-level *h*-BN domains which only consisted of the B-N bonding modes were *in situ* generated and embedded into the hexagonal plane of graphene matrix with formation of BN-graphene boundaries;[7,24] (3) a mixture of *h*-BN bulk and graphene as well as a layer-by-layer composite could also be formed because B-N and C-C bonds tended to segregate from each other.[17] To date, it has remained a challenging task to control the doping patterns formed by B and N atoms and especially to obtain atomic-level *h*-BN domains generated in graphene *via* facile and controllable doping strategy. Furthermore, the application of the *h*-BN domains decorated graphene in photocatalytic hydrogen generation has rarely been reported in the literature, not to mention the possible structure-property relationship for this *h*-BN doped graphene catalyst.

By regulating the order of heteroatom doping (a stepwise doping strategy) and the oxygen content of graphene precursor, we report herein a precise synthesis of the graphene decorated with in-plane *h*-BN domains (donated as BN-G), B and N single-doped graphene (denoted as B-G and N-G, respectively), and B, N co-doped graphene (denoted as B,N-G). The formation of in-plane *h*-BN domains in graphene was carefully characterized by X-ray photoelectron spectroscopy (XPS) and IR spectra. In comparison to the conventional CVD method, our chemical doping strategy for the preparation of BN-G is much more facile and promising for the large-scale application. When applied in photocatalytic hydrogen generation, the BN-G photocatalyst exhibited a significant increase (*ca*. 10-fold) in the hydrogen production rate compared with other B

and/or N doped graphene photocatalysts. Density functional theory (DFT) calculations validate that our stepwise doping strategy was effective in controlling the doping patterns of heteroatoms in graphene for finely engineering their band structures and related photocatalytic properties.

EXPERIMENTAL SECTION

Preparation of B-G, N-G, B,N-G and BN-G. Graphene oxide (GO) and graphene (G) were synthesized according to the previously reported method by our group.[25] Boric acid (A.R.) and ethanol (A.R.) were purchased from Beijing Chemical Works. Boron nitride bulk (99%) was purchased from J&K Chemicals. H_2 (99.999%) and ammonia (99%) were purchased from Beijing Haikeyuanchang Gas Co., Ltd. The synthetic processes of N-GO, B-G, N-G, B,N-G and BN-G were summarized in Figure S1 (Supporting Information). N-GO was synthesized by calcining graphene oxide at 500 ^{o}C for 4 h under 10 mL min^{-1} NH_3 flow. B-G was obtained as follows: Graphene was incipient wetness impregnated with boron acid dissolved in ethanol. The amount of boron acid respect to graphene was decided by fixing the B/C ratio to be 15/100. The mixture was dried under the infrared lamp and then dried in drum wind drying oven at 60 ^{o}C for 6h to remove ethanol. Then the solid was calcined at 900 ^{o}C for 6 h under 40 mL min^{-1} H_2 flow. N-G was obtained as follows: Graphene oxide was calcined at 500 ^{o}C for 4 h under 40 mL min^{-1} H_2 flow, then was calcined at 900 ^{o}C for 6 h under 10 mL min^{-1} NH_3 flow. B,N-G was obtained as follows: N-GO was incipient wetness impregnated with boron acid dissolved in ethanol. The amount of boron acid respect to graphene was decided by fixing

the B/C ratio to be 15/100. The mixture was dried under the infrared lamp and then dried in drum wind drying oven at 60 ^{o}C for 6 h to remove ethanol. Then the solid was calcined at 900 ^{o}C for 6 h under 40 mL min^{-1} H_2 flow. BN-G was obtained as follows：Graphene was incipient wetness impregnated with boron acid dissolved in ethanol. The amount of boron acid respect to graphene was decided by fixing the B/C ratio to be 15/100. The mixture was dried under the infrared lamp and then dried in drum wind drying oven at 60 ^{o}C for 6 h to remove ethanol. Then the obtained solid was calcined at 900 ^{o}C for 6 h under a mixture flow of 40 mL/min H_2 and 10 mL min^{-1} NH_3.

Materials characterization. UV-Vis absorbance spectra were recorded on a Cary 5000 spectrometer. Fourier transform infrared spectroscopy **(**FT-IR) measurement was performed on a Spectrum Spotlight 200 FT-IR microscopy from PE. Raman measurements were performed under ambient conditions using a 532 nm (2.33 eV) laser in the back-scattering configuration on a Jobin-Yvon HR800 spectrometer. Transmission electron microscope (TEM) images were obtained with a JEOL JEM-2010 microscope operated at an accelerating voltage of 120 kV. Scanning transmission electron microscopy (STEM) characterizations were conducted by using FEI Talos F200X equipped with Super-X EDX, operating at 200kV. X-ray photoelectron spectroscopy (XPS) analysis was taken on an Axis-Ultra instrument from Kratos Analytical Ltd. using monochromatic Al Kα radiation (225 W, 15 mA, 15 kV). Electron spin resonance (ESR) spectra were collected on a Bruker 500. The periodic on/off photocurrent response for photocatalysts was obtained under UV-vis irradiation by loading catalysts (~1 mg catalysts dispersed in methanol) on ITO glass (1*1 cm^2).

Photocatalytic performance test. 3 mg doped graphene catalyst was added into a 130

mL quartz reactor containing 50 ml 10% TEOA solution and 3 wt% Pt. The Pt precursor was $H_2PtCl_6 \cdot 6H_2O$. The slurry was stirred vigorously and sonicated to achieve a homogeneous dispersion. Then, the reactor was covered by a quartz lid, sealed and purged for 30 min with argon and irradiated under a 300 W xenon light source (Newport 66485-300XF-R1) for 1 hour as the photodeposition period. During this period, we took GC measurements every 15 mins by a gas tight syringe until the gas evolution rate was stable, which indicated that the photodeposition was complete. After the photodepostion, the reactor was purged for the second time for 30 min with argon and irradiated under the same 300 W light source. GC measurements were taken every hour to record the generated H_2 amount. The long-term stability of the BN-G has also been assessed for 24 h with each cycle for 4 h. Before starting each cycle, the quartz reactor was purged with argon for 30 min. The apparent quantum efficiency (QE) was tested under irradiation of a 300 W Xenon light source equipped with 380 nm, 420 nm, 500 nm, and 600 nm band pass filters, respectively. The band pass filter has a bandwidth of ± 5 nm. QE was calculated according to the following equation:

$$\mathrm{QE}[\%] = \frac{number\ of\ reacted\ electrons}{number\ of\ incident\ photons} \times 100$$
$$= \frac{number\ of\ evolved\ H_2\ molecules \times 2}{number\ of\ incident\ photons} \times 100$$

Computational methods. Plane-wave density functional theory (DFT) calculations of the electronic properties of G, N-G, B-G, B,N-G, and BN-G were carried out using CASTEP module in Material Studio. The generalized calculation details were the same as those reported in our previous paper.[26] In briefly, the generalized gradient approximation (GGA) with Perdew-Burke-Ernzerhof (PBE) functional was employed for the DFT

exchange correlation energy, and 340 eV of cutoff was assigned to the plane-wave basis set. The self-consistent field (SCF) tolerance was 1×10^{-6} eV. The Brillouin zone was sampled by 1×1×2 k-points. The core electrons were replaced with ultrasoft pseudo-potentials.

RESULTS AND DISCUSSION

The synthetic processes for representative heteroatom-doped graphene (BN-G and B,N-G) are illustrated in Figure 1. Ammonia (NH_3) and boron acid (H_3BO_3) were selected as the precursors of N and B atoms during the syntheses of these graphene catalysts, respectively. The doping of heteroatoms was considered to easily undergo a substitution reaction between the dopant (*i.e.* B or N) and the C atoms in graphene precursor due to their similar atomic diameters.[17] However, it should be noted that the oxygen content in precursor is critical for affecting the doping level of N atoms, as oxygen groups in GO were responsible for reactions with NH_3, leading to the formation of C-N bond. Pre-reducing GO by thermal annealing in H_2 (to remove oxygen groups) exhibits reduced reactivity with NH_3 and thereby a lower N-doping level in the resulted sample.[27] Therefore, N-GO with a high oxygen content was synthesized by a one-step calcination in NH_3 at 500 ^oC, while N-G was obtained by firstly subjecting GO in flowing H_2 at 500 ^oC to lower its oxygen content and then calcining in NH_3 at 900 ^oC. As shown in Figure 1, B,N-G was obtained by using N-GO as the precursor to form a mixture with H_3BO_3, followed with a calcination in H_2. G with relatively lower oxygen content was obtained from the reduction of GO under H_2 atmosphere and employed as the precursor for B-G and BN-G (Figure 1). The doping of B in graphene (B-G) was accomplished by calcining the mixture of H_3BO_3 and graphene in flowing H_2 at 900 ^oC. We reasoned that

the leaving of oxygen groups in graphene at high temperature provides defects (active sites) that favor the B doping.[28] Notably, BN-G can be achieved by the identical method to that of B-G except mixing a certain amount of NH_3 in the H_2 flow during the calcination process. Here, the doping processes were conducted under H_2 atmosphere in order to further remove the oxygen groups in graphene, whereby the influence of B and N doping on the band gap engineering of graphene can be assessed except the effect of oxygen species. It should be noted that the doping configurations of B and N atoms and *h*-BN domains in graphene are believed to be substitutional doping, that is, carbon atoms in the sp^2 network of graphene are substituted by corresponding B, N or *h*-BN after doping.[7,17]

The formation of *h*-BN domains in graphene could be explained by two reasons: one is that the separate doping of N and B atoms into graphene could be inhibited due to the relative lower oxygen content in the precursor;[27] the other could be that the bond energy of B-N is higher than that of C-N, so N has a stronger tendency to bond with B than to bond with C.[7,29] G (with 1.5% oxygen) contained defects which were formed from the leaving of oxygen groups during GO reduction. These defects provide the active sites for B-doping.[28] On the other hand, the decrease of the oxygen content in G can inhibit the reaction with NH_3 and the subsequent C-N bond formation. Also, due to the binding energy of B-N is higher than that of C-N, N has a stronger tendency to bond with B than to bond with C, making the formation of BN domains straightforward. It is worth noting that the doping order of B and N is very important for the formation of BN in graphene. In our case, it is speculated that a uniformly dispersed boron species on the surface of G could trigger the B-doping prior to the N-doping under H_2/NH_3 atmosphere,

which would favor the formation of BN domains because it is easier for NH_3 to bond with doped B to form BN instead of the separate N-doping. However, if we change the doping step to first treating with NH_3 for N-doping and then impregnating N-GO with boron acid, B,N-G will be formed because H_3BO_3 is solid and tends to react with dominant C atoms. In addition, the concentration of doped BN was controlled, as bulk BN will be formed if the BN concentration is higher than a certain value,[7] which could lead to the segregation of BN from graphene matrix.

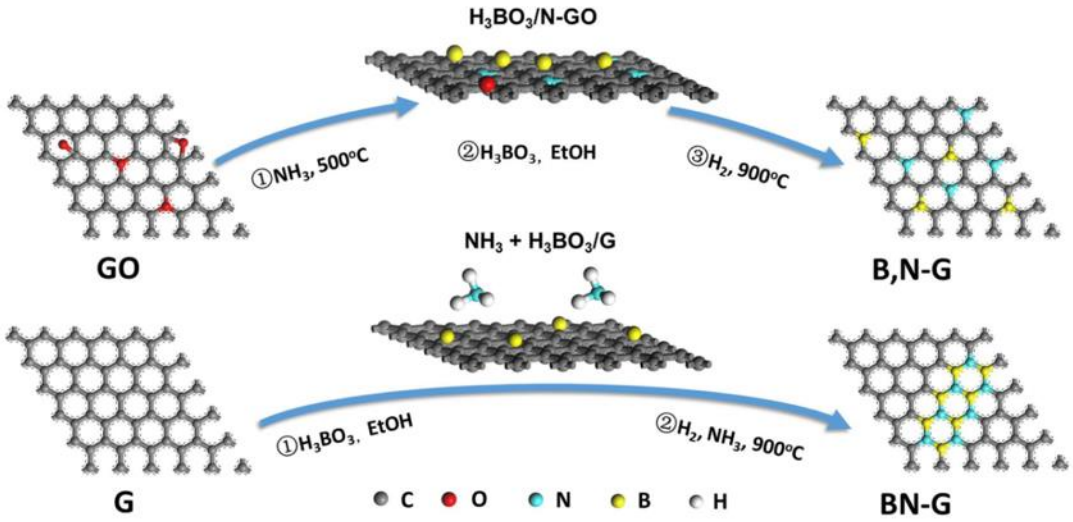

Figure 1. Schematic diagram of the synthetic processes for the B, N co-doped grapheme (B,N-G) and graphene decorated with *h*-BN domains (BN-G).

The surface structure and morphology of pristine and heteroatom-doped graphene samples were characterized by transmission electron microscopy (TEM) (Figure 2A, 2B, Figure S2). All the heteroatom-doped graphene materials exhibited nearly intact sheet-like structures, which were very similar to pristine graphene (Figure S2A), demonstrating that the doping of B and/or N atoms would not destroy the graphene nanostructures. It was also observed that both B,N-G and BN-G samples only contained

wrinkled graphene sheets with a thickness of 1-2 layers without formation of any out-of-plane layered structures or bulk composites (Figure 2A, 2B), furthermore, high angle annular dark field-scanning transmission electron microscopy (HAADF-STEM) image of BN-G was further recorded to analyze the atomic-level structure (Figure 2C-F and Figure. S3). There was no obvious bulk BN formation, and the EDX mapping image of N indicated that N atoms were dispersed uniformly in graphene in very small regions of a few square nanometers. The B element signal was so weak that we could not obtain a clear mapping image of B, possibly due to the limitation of the EDX detector. All the above data suggest the homogeneous doping of heteroatoms in these graphene samples. The differences in the doping patterns formed by B and N atoms between B,N-G and BN-G could not be directly observed in TEM images. The detailed structure of *h*-BN domains in graphene will be further discussed below.

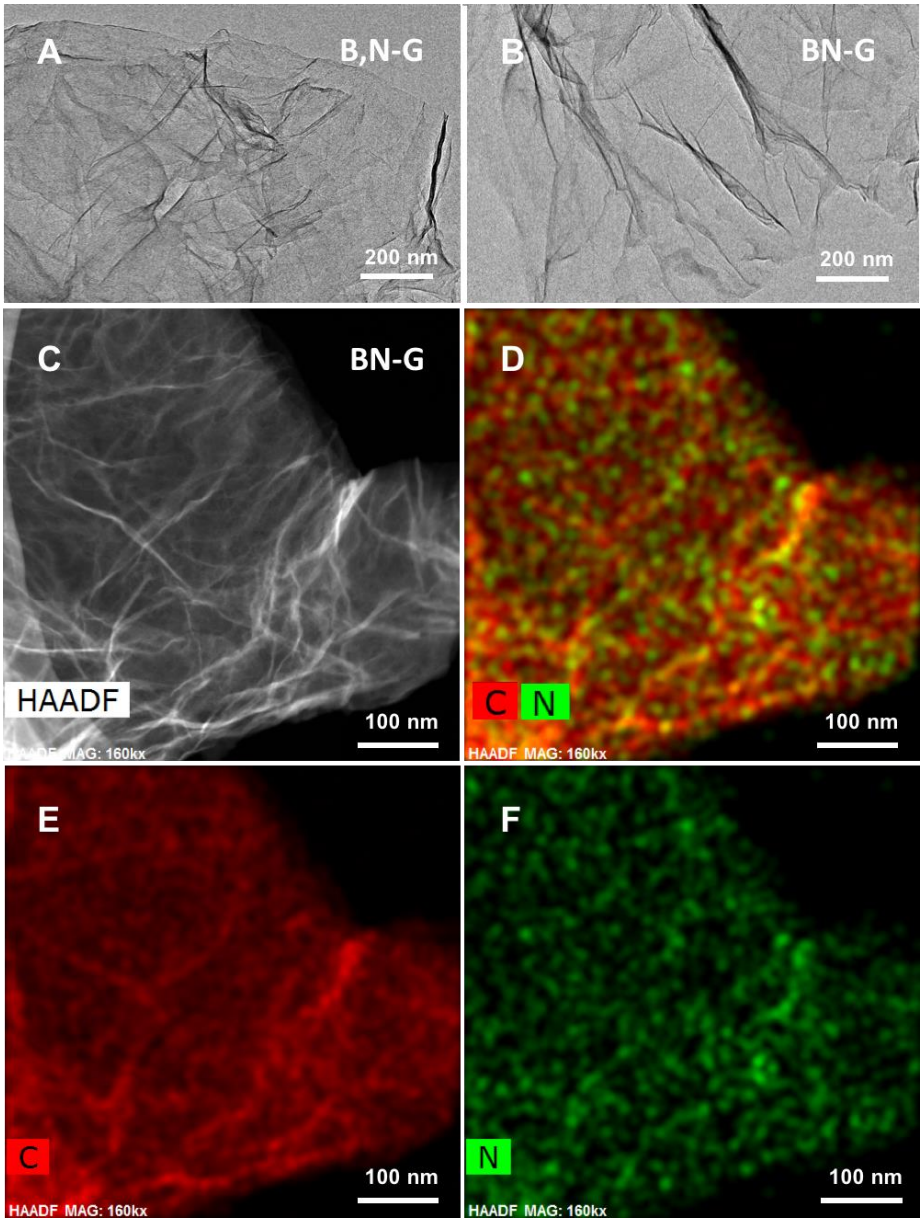

Figure 2. Typical TEM images of (A) B,N-G, (B) BN-G. The HAADF-STEM image (C) and corresponding EDX mapping images for (D) C and N elements, (E) C elements and (F) N elements of BN-G.

To further reveal the surface elemental composition and the nature of doping pattern of B and N atoms in the heteroatom-doped graphene, we conducted X-ray photoelectron spectroscopy (XPS) measurements. The elemental compositions for the

pristine and doped graphene samples were summarized in Table S1. The pristine graphene only contained 98.5 at% C and 1.5 at% O in the surface in the absence of B and N elements. After doping with heteroatoms, 2.2 at% B, 3.4 at% N and 4.0 at% N were detected in B-G, N-G, and N-GO, respectively. Moreover, both B and N atoms can be detected in B,N-G and BN-G, suggesting the successful co-doping of these two elements in graphene, which will be further discussed. The BN-G contained very similar atomic percentages of B (4.8 at%) and N (4.3 at%) atoms, approaching that of an optimized BN-doped graphene containing 6% BN domains.[20] Although we try to keep the B/C and N/C ratios the same, some deviation was introduced due to the uncontrollable factors during the impregnation and calcination process. The difference in the doping patterns between B,N-G and BN-G was revealed by the high resolution XPS spectra of B 1s and N 1s. As shown in Figure 3A, BN-G exhibits the similar main peak of B 1s to BN powder, which may suggest the successful formation of *h*-BN domains in graphene. Besides, a slight tail of B 1s peak in higher binding energies could be attributed to the formation of B-C bonds at the boundary of *h*-BN domains and graphene.[20,29] The N 1s XPS spectrum of BN-G gives the same trend to that of B 1s spectrum, also indicating the presence of *h*-BN domains in BN-G (Figure 3B). The B 1s and N 1s peaks of B,N-G were significantly different from the BN power and BN-G but quite similar to the single-doped B-G, N-G and N-GO, which implied that the B and N atoms were separately doped into graphene without formation of *h*-BN domains. Further evidences were collected from IR spectra of BN powder and B and/or N doped graphene samples (Figure 3C). For BN-G, in addition to the C-C bond vibrations at around 1220 and 1550 cm^{-1}, strong B-N bond vibrations at around 800 and 1380 cm^{-1} can also be observed in its

IR spectrum, which is similar to that of BN powder. However, no obvious B-N vibration peaks were detected in B-G, N-G, N-GO and B,N-G samples. In line with the XPS results, the IR data again suggested that the *h*-BN domains were generated in graphene for BN-G, while B and N atoms were separately doped for B,N-G. Combining with the observation of simple graphene structures without any BN layers or bulks from TEM images, the characteristic features of B-N bonding modes from XPS and IR spectra, as well as the similar atomic percentages of B and N atoms in BN-G, we are able to conclude that our controlled doping strategy has succeeded in achieving atomic-level in-plane decoration of *h*-BN domains in graphene. According to previous studies, this *in situ* formed *h*-BN domains would have great effects on the structural and electronic properties of graphene compared with the B and/or N single- or co-doping into graphene.

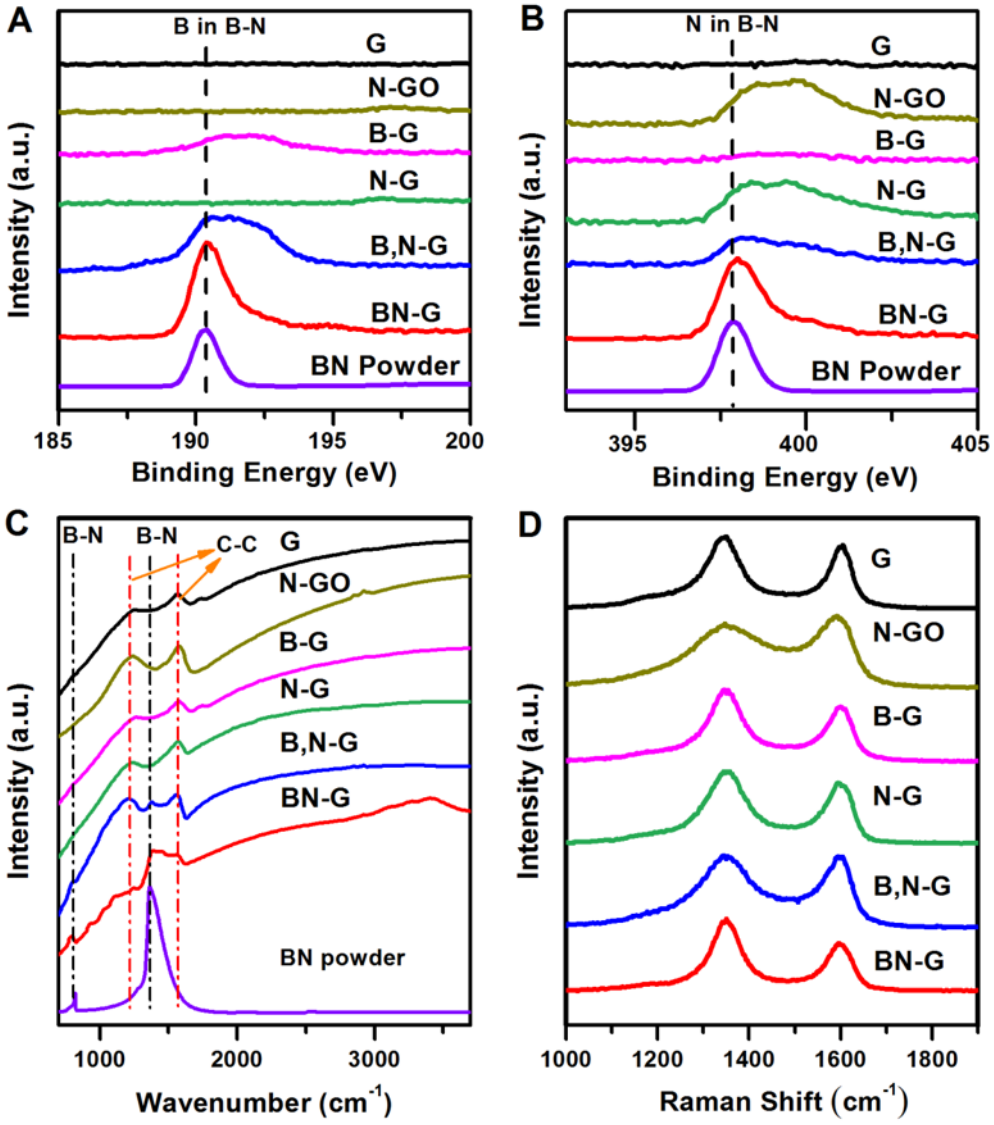

Figure 3. High resolution B 1s (A) and N 1s (B) XPS spectra, IR spectra (C) and Raman spectra (D) of BN powder, pristine and heteroatom-doped graphene materials.

We further employed the Raman spectra of the doped graphene samples to explore the differences in carbon nanostructures after doping with B and N. As shown in Figure 3D, two main signals namely D band located at around 1350 cm^{-1} and G band around 1600 cm^{-1} were clearly observed for all samples, corresponding to the distorted

and graphitic carbon structures, respectively. The intensity ratio of D band to G band (I_D/I_G) can reflect the degree of structural disorder in graphene (Table S2).[30] The I_D/I_G of G (1.20) is much higher than that of GO (0.87), mainly due to the increased amount of defects during GO reduction. The I_D/I_G of N-G (1.16) is close to G (1.20) and also higher than GO (0.87), possibly due to that formation of defects is predominant during the calcination over N-doping. In contrast, the I_D/I_G of N-GO (0.91) is lower than G and N-G, because N-doping process at a mild temperature (500 ^oC) can meanwhile repair some defects of GO. After B-doping, both B-G and B,N-G showed slight increases in I_D/I_G compared with their precursors, *i.e.* G and N-GO, respectively. This is because that the electron deficiency of B atoms would lead to *n*-type substitutional doping and create more defects in graphene. It is noteworthy that BN-G displays the highest I_D/I_G value (1.53) among these samples, indicating a much less proportion of graphitic carbon structures in graphene framework of BN-G. This is reasonable because the doping of *h*-BN domains (insulator) would substitute the sp^2 carbon structures without providing delocalized π electrons for maintaining the π-π conjugated network of graphene.[31] The distortions in graphene could be favorable for modifying the band gap and creating new active sites. Figure 4A shows the UV-Vis spectra of our graphene-based samples, it is found that all the samples have the UV-Vis absorption capabilities. In our experiment, graphene was obtained from reduction of GO. Although it is mixed-layered graphene at the micro level, but at the macro level it is black fluffy solid with a strong UV-Vis absorption over the whole wavelength range. Thereby, the present data strongly demonstrate that the graphene decorated with *h*-BN domains can be anticipated as a promising candidate for efficiently harvesting and utilizing the solar energy.

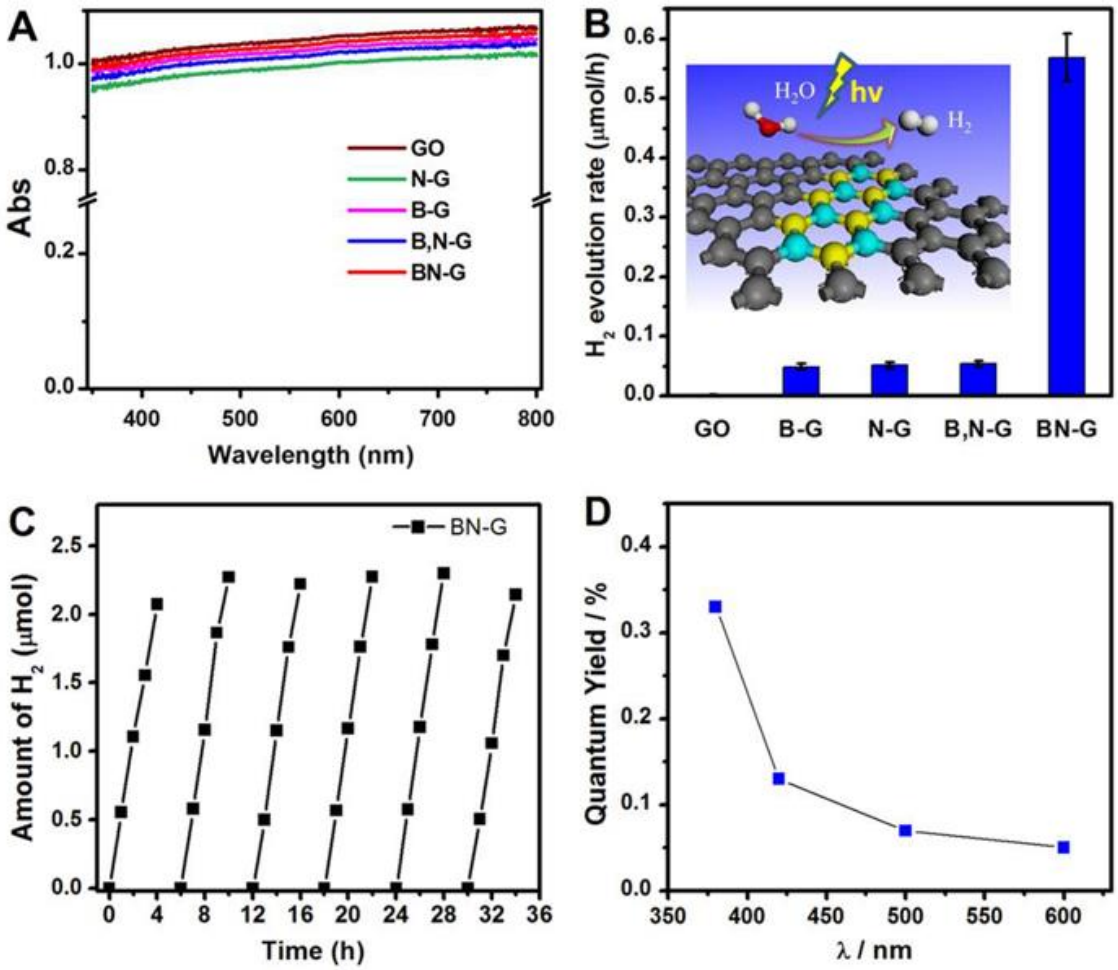

Figure 4. (A) UV-Vis spectra of heteroatom-doped graphene photocatalysts. (B) Hydrogen production activity of GO, B-G, N-G, B,N-G and BN-G in photocatalytic hydrogen evolution (Inset is the schematic of hydrogen evolution from water on the surface of BN-G). (C) Stability of BN-G in photocatalytic hydrogen evolution. (D) Apparent quantum yield of BN-G in 380 nm, 420 nm, 500 nm and 600 nm.

The unique structural and electronic properties resulted from the atomic-level decoration of *h*-BN domains inspired us to investigate the potential application of BN-G in photocatalytic hydrogen generation and the related structure-property relationship. Here, we tested the hydrogen evolution rate of the as-obtained GO, B-G, N-G, B,N-G,

and BN-G in aqueous solution containing 10% triethanolamine (TEOA) as sacrificial agent under UV-Vis light irradiation (Figure 4B). Before each test, 3 wt% platinum was photodeposited on these graphene materials as the co-catalyst to promote the separation of photoelectrons for hydrogen evolution. As shown in Figure 4B, the pristine GO showed no detectable activity, possibly due to its relatively low oxygen content (ca. 18 wt%) and thus insufficient band gap (< 1.0 eV).[32,33] After doping with heteroatoms, the B-G, N-G and B,N-G all exhibited certain activities for hydrogen evolution with a rate of 0.045-0.055 μmol h^{-1}. The very similar H_2 evolution rates between these catalysts may suggest that the doping modes of heteroatoms are similar to each other, supporting our above conclusion that B and N were separately doped in these catalysts with homogeneous heteroatom distributions. Remarkably, BN-G showed a 10-fold increase in H_2 evolution rate (*ca.* 0.57 μmol h^{-1}) compared with single- and co-doped graphene catalysts (N-G, B-G, and B,N-G). This result demonstrates that the *h*-BN doping strategy is highly efficient for enhancing the H_2 evolution activity. In addition, the long-term stability of BN-G in the photocatalytic process was assessed by cycling the catalyst for 24 h under UV-Vis light irradiation. As shown in Figure 4C, the H_2 production rate can be well maintained around 0.57 μmol h^{-1} during the stability test, suggesting that BN-G was very stable in photocatalytic process and could be highly promising for practical applications. The apparent quantum yields (QY) of the BN-G for hydrogen evolution at different light wavelengths were also calculated, as shown in Figure 4D. A QY of 0.3 % was obtained for BN-G under monochromatic irradiation at 380 nm. BN-G also showed obvious visible-light-induced hydrogen evolution activity. During the photocatalytic process, both the photoexcited holes and electrons from the conductive and valance bands

of BN-G were detected by electron spin resonance (ESR) spectra (Figure 5A, B), respectively, as follows:

$$h\nu + \text{BN-G} \rightarrow \text{BN-G}\ (e_{CB}^{-} + h_{VB}^{+}) \quad (1)$$

$$e_{CB}^{-} + O_2 \rightarrow O_2^{\bullet -} \quad (2)$$

$$h_{VB}^{+} + OH^{-} \rightarrow {}^{\bullet}OH \quad (3)$$

This provided a solid indication that the photogenerated charge carriers in BN-G gave strong redox ability during the photocatalytic H_2 evolution process. Furthermore, according to I-T curves (Figure 5C), the improved charge separation efficiency of BN-C leads to an increased photocurrent density compared with B,N-C and G without obvious band gap. The above results conclusively demonstrate that BN-C shows improved separation efficiency of photogenerated charges, which are key factors that contribute to the exceptional photocatalytic hydrogen generation activity.

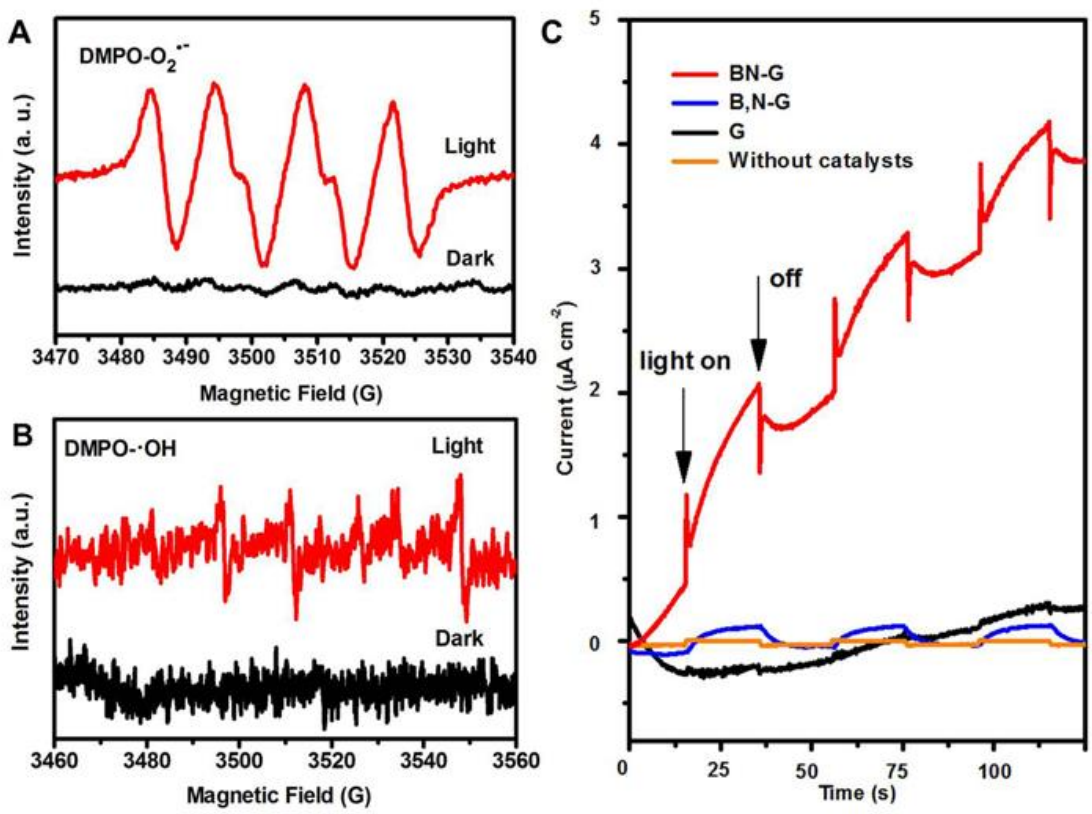

Figure 5. ESR spectra recorded on BN-G for detection of (A) $O_2^{\bullet-}$ radicals in methanol dispersion, and (B) $^{\bullet}OH$ radicals in aqueous dispersion by using 5,5-dimethyl-1-pyrroline-N-oxide (DMPO) under UV-Vis light, (C) the periodic on/off photocurrent response for BN-G, B,N-G, G and without any catalysts deposited on ITO glass under UV-vis irradiation.

The above results have confirmed that in-plane decoration of *h*-BN domains into graphene can greatly affect the surface structure and catalytic activity of graphene-based catalyst. To further study the electronic property of BN-G (*e.g.* band gap) and the structure-property relationship, Density functional theory (DFT) calculations were conducted to examine the band structure, the densities of states (DOS), as well as the partial densities of states (PDOS) for heteroatom-doped graphene systems. The atomic

structure models of BN-G and other graphene catalysts are shown in Figure 6A and Figure S4. The band structure of BN-G shown in Figure 6B indicates that the top of the valence band and the bottom of the conduction band are mainly composed of *p*-orbitals and are co-contributed by C, B, and N atoms. All of the B and N atoms have covalence interactions with C atoms, which contribute to the corresponding bandgap. The band structure and DOS around the Fermi level of BN-G were calculated to give a band gap of *ca.* 2.8 eV (Figure 6B-C). Compared with BN-G, the band gaps of GO, B-G, N-G and B,N-G were quite narrow (0-1.4 eV) while the band gap of *h*-BN bulk was too large (*ca.* 4.8 eV) (Figure 6D, Figure S5). The very similar band gap opening of B-G, N-G, and B,N-G arises from the similar doping pattern and concentrations of dopant (B: 2.2 - 5.3%, N: 2.4 - 4.3%).[34] The doping pattern in B,N-G can be regarded as a random mixture of the doped B atoms in B-G and N atoms in N-G. In contrast, the doping pattern in BN-G is completely different from B,N-G, involving the embedment of *h*-BN domains into graphene by substituting sp^2 carbon network. As we know, BN is an insulator while graphene is a semi-metal. After embedding in G, BN-G turns to be a semiconductor with a larger band gap, possibly due to the significant shrink in the π-π conjugated network of graphene.[31] The unique doping pattern in BN-G is anticipated as the main reason for the band gap opening. It is well known, either too large or too small band gap would be unable to efficiently utilize the light energy. Because of the suitable band gap of BN-G by introduction of *h*-BN domains, the light absorption ability and electric conductivity can be improved and the valence electrons can be easily excited and transferred to H_2O molecules for H_2 evolution. Thereby, our controlled doping strategy for achieving various doping modes involving B and N atoms could effectively modify the structure and band

gap of graphene, which are responsible for varied photocatalytic activities in hydrogen generation. Furthermore, through calculating the location of the Fermi level relative to valance band maximum (VBM) (Figure S6, S7), the energy level of conductive band minimum (CBM) and VBM relative to the vacuum level of graphene-based catalysts was obtained and listed in Table S3. As shown in Figure S8, the CBM of BN-G gives more negative potential compared with B-N, N-G and B,N-G, further indicating its stronger ability to produce photogenerated electrons for the H_2 evolution from H_2O. This understanding on the structure-property relationship may pave the way for the rational design of active photocatalysts on the molecular level.

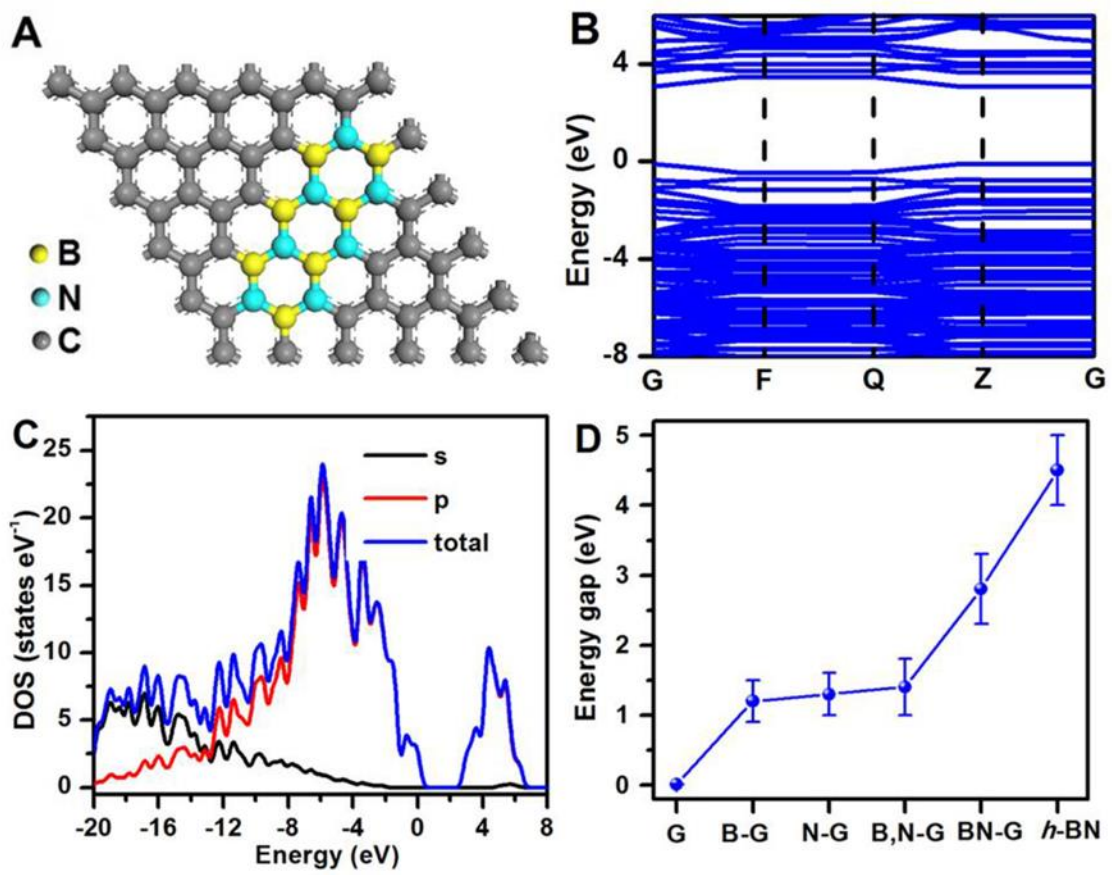

Figure 6. Atomic structure model (A); band structure (B); total and partial electronic density of states (TDOS and PDOS) (C) for BN-G. The Fermi level is set at 0 eV. (D) Calculated band gaps of G, B-G, N-G, B,N-G, BN-G and *h*-BN.

CONCLUSION

In summary, this work uncovers that not only the doping of B and N atoms but also the doping patterns formed by these heteroatoms can affect the structural and electronic properties of graphene and its photocatalytic activity in H_2 evolution. The *in situ* formation of atomic-level *h*-BN domains in graphene is found to be critical for engineering the band structure to create an optimal band gap that can efficiently utilize solar energy, further enhancing its photocatalytic performance. This *h*-BN doping

strategy would inspire more studies in seeking for novel doping patterns (or structures) and tuning their semiconductor properties for replacing graphene in constructing high active photocatalysts for energy-related applications.

ASSOCIATED CONTENT

Supporting Information.

The Supporting Information is available free of charge on the ACS Publications website.

Materials synthesis, extended characterization results, including TEM, HAADF-STEM, XPS, Raman, DFT results (PDF).

AUTHOR INFORMATION

Corresponding Author

* dma@pku.edu.cn

* yufei.zhao@mail.ipc.ac.cn

Author Contributions

All authors have given approval to the final version of the manuscript.

ACKNOWLEDGMENT

This work was financially supported by the Natural Science Foundation of China (91645115，21473003, 21401206, 21673273) and 973 Project (2013CB933100).

REFERENCE

(1) Fan, X.; Zhang, G.; Zhang, F. Multiple Roles of Graphene in Heterogeneous Catalysis. *Chem. Soc. Rev.* **2015**, 44, 3023-3035.

(2) Xie, G.; Zhang, K.; Guo, B.; Liu, Q.; Fang, L.; Gong, J. R. Graphene-Based Materials for Hydrogen Generation from Light-Driven Water Splitting. *Adv. Mater.* **2013**, 25, 3820-3839.

(3) Zhang, N.; Zhang, Y. H.; Xu, Y. J., Recent Progress on Graphene-Based Photocatalysts: Current Status and Future Perspectives. *Nanoscale* **2012**, 4, 5792-5813.

(4) Lin, T.; Huang, F.; Liang, J.; Wang, Y. A Facile Preparation Route for Boron-Doped Ggraphene, and Its CdTe Solar Cell Aapplication. *Energy Environ. Sci.* **2011**, 4, 862-865.

(5) Cao, A.; Liu, Z.; Chu, S.; Wu, M.; Ye, Z.; Cai, Z.; Chang, Y.; Wang, S.; Gong, Q.; Liu, Y. A Facile One-step Method to Produce Graphene–CdS Quantum Dot Nanocomposites as Promising Optoelectronic Materials. *Adv. Mater.* **2010**, 22, 103-106.

(6) Dong, C.; Li, X.; Jin, P.; Zhao, W.; Chu, J.; Qi, J. Intersubunit Electron Transfer (IET) in Quantum Dots/Graphene Complex: What Features Does IET Endow the Complex with? *J. Phys. Chem. C* **2012**, 116, 15833-15838.

(7) Ci, L.; Song, L.; Jin, C.; Jariwala, D.; Wu, D.; Li, Y.; Srivastava, A.; Wang, Z. F.; Storr, K.; Balicas, L.; Liu, F.; Ajayan, P. M. Atomic Layers of Hybridized Boron Nitride and Graphene Domains. *Nat. Mater.* **2010**, 9, 430-435.

(8) Yeh, T. F.; Syu, J. M.; Cheng, C.; Chang, T. H.; Teng, H. Graphite Oxide as a Photocatalyst for Hydrogen Production from Water. *Adv. Funct. Mater.* **2010**, 20, 2255-2262.

(9) Yeh, T. F.; Chan, F. F.; Hsieh, C. T.; Teng, H. Graphite Oxide with Different

Oxygenated Levels for Hydrogen and Oxygen Production from Water under Illumination: The Band Positions of Graphite Oxide. *J. Phys. Chem. C* **2011**, 115, 22587-22597.

(10) Putri, L. K.; Ong, W. J.; Chang, W. S.; Chai, S. P. Heteroatom Doped Graphene in Photocatalysis: A Review. *Appl. Surf. Sci.* **2015**, 358, 2-14.

(11) Kakaei, K.; Balavandi, A. Synthesis of Halogen-Doped Reduced Graphene Oxide Nanosheets as Highly Efficient Metal-Free Electrocatalyst for Oxygen Reduction Reaction. *J. Colloid. Interf. Sci.* **2016**, 463, 46-54.

(12) Latorre-Sánchez, M.; Primo, A.; García, H. P-Doped Graphene Obtained by Pyrolysis of Modified Alginate as a Photocatalyst for Hydrogen Generation from Water-Methanol Mixtures. *Angew. Chem., Int. Ed.* **2013**, 52, 11813-11816.

(13) Lavorato, C.; Primo, A.; Molinari, R.; Garcia, H. N-Doped Graphene Derived from Biomass as a Visible-Light Photocatalyst for Hydrogen Generation from Water/Methanol Mixtures. *Chem. Eur. J.* **2014**, 20, 187-194.

(14) Yeh, T. F.; Chen, S. J.; Yeh, C. S.; Teng, H. Tuning the Electronic Structure of Graphite Oxide through Ammonia Treatment for Photocatalytic Generation of H_2 and O_2 from Water Splitting. *J. Phys. Chem. C* **2013**, 117, 6516-6524.

(15) Zheng, Y.; Jiao, Y.; Ge, L.; Jaroniec, M.; Qiao, S. Z. Two-Step Boron and Nitrogen Doping in Graphene for Enhanced Synergistic Catalysis. *Angew. Chem,. Int. Ed.* **2013**, 52, 3110-3116.

(16) Kim, I. T.; Song, M. J.; Kim, Y. B.; Shin, M. W. Microwave-Hydrothermal Synthesis of Boron/Nitrogen co-doped Graphene as an Efficient Metal-Free Electrocatalyst for Oxygen Reduction Reaction. *Int. J. Hydrogen. Energy*. **2016**, 41, 22026-22033.

(17) Song, L.; Liu, Z.; Reddy, A. L. M.; Narayanan, N. T.; Taha-Tijerina, J.; Peng, J.; Gao, G.; Lou, J.; Vajtai, R.; Ajayan, P. M. Binary and Ternary Atomic Layers Built from Carbon, Boron, and Nitrogen. *Adv. Mater.* **2012**, 24, 4878-4895.

(18) Lim, H.; Yoon, S. I.; Kim, G.; Jang, A. R.; Shin, H. S. Stacking of Two-Dimensional Materials in Lateral and Vertical Directions. *Chem. Mater.* **2014**, 26, 4891-4903.

(19) Zhang, J.; Xie, W.; Xu, X.; Zhang, S.; Zhao, J. Structural and Electronic Properties of Interfaces in Graphene and Hexagonal Boron Nitride Lateral Heterostructures. *Chem. Mater.* **2016**, 28, 5022-5028.

(20) Chang, C. K.; Kataria, S.; Kuo, C. C.; Ganguly, A.; Wang, B. Y.; Hwang, J. Y.; Huang, K. J.; Yang, W. H.; Wang, S. B.; Chuang, C. H.; Chen, M.; Huang, C. I.; Pong, W. F.; Song, K. J.; Chang, S. J.; Guo, J. H.; Tai, Y.; Tsujimoto, M.; Isoda, S.; Chen, C. W.; Chen, L. C.; Chen, K. H. Band Gap Engineering of Chemical Vapor Deposited Graphene by in Situ BN Doping. *ACS Nano* **2013**, 7, 1333-1341.

(21) Ma, R.; Bando, Y.; Sato, T. Controlled Synthesis of BN Nanotubes, Nanobamboos, and Nanocables. *Adv. Mater.* **2002**, 14, 366-368.

(22) Kubota, Y.; Watanabe, K.; Tsuda, O.; Taniguchi, T. Deep Ultraviolet Light-Emitting Hexagonal Boron Nitride Synthesized at Atmospheric Pressure. *Science* **2007**, 317, 932-934.

(23) Song, X.; Gao, T.; Nie, Y.; Zhuang, J. Seed-Assisted Growth of Single-Crystalline Patterned Graphene Domains on Hexagonal Boron Nitride by Chemical Vapor Deposition. *Nano. Lett.* **2016**, 16, 6109–6116.

(24) Han, W.; Bando, Y.; Kurashima, K.; Sato, T. Synthesis of Boron Nitride Nanotubes

from Carbon Nanotubes by a Substitution Reaction. *Appl. Phys. Lett.* **1998**, 73, 3085-3087.

(25) Tang, P.; Hu, G.; Gao, Y. The Microwave Adsorption Behavior and Microwave-Assisted Heteroatoms Doping of Graphene-Based Nano-Carbon Materials. *Sci. Rep.* **2013**, 4, 5901.

(26) Zhao, Y.; Zhang, S.; Li, B. A Family of Visible-Light Responsive Photocatalysts Obtained by Dispersing CrO_6 Octahedra into a Hydrotalcite Matrix. *Chem. Eur. J.* **2011**, 17, 13175-13181.

(27) Li, X.; Wang, H.; Robinson, J. T.; Sanchez, H.; Diankov, G.; Dai, H. Simultaneous Nitrogen Doping and Reduction of Graphene Oxide. *J. Am. Chem. Soc.* **2009**, 131, 15939-15944.

(28) Sheng, Z. H.; Gao, H. L.; Bao, W. J.; Wang, F. B.; Xia, X. H. Synthesis of Boron Doped Graphene for Oxygen Reduction Reaction in Fuel Cells. *J. Mater. Chem.* **2012**, 22, 390-395.

(29) Han, W. Q.; Yu, H. G.; Liu, Z. Convert Graphene Sheets to Boron Nitride and Boron Nitride–Carbon Sheets via a Carbon-Substitution Reaction. *Appl. Phys. Lett.* **2011**, 98, 203112-203114.

(30) Choi, C. H.; Chung, M. W.; Kwon, H. C.; Park, S. H.; Woo, S. I. B, N- and P, N-Doped Graphene as Highly Active Catalysts for Oxygen Reduction Reactions in Acidic Media. *J. Mater. Chem. A* **2013**, 1, 3694-3699.

(31) Gong, Y.; Shi, G.; Zhang, Z.; Zhou, W.; Jung, J.; Gao, W.; Ma, L.; Yang, Y.; Yang, S.; You, G.; Vajtai, R.; Xu, Q.; MacDonald, A. H.; Yakobson, B. I.; Lou, J.; Liu, Z.; Ajayan, P. M. Direct Chemical Conversion of Graphene to Boron- and Nitrogen- and

Carbon-Containing Atomic Layers. *Nat. Commun*. **2014**, 5, 3193-3200.

(32) Huang, H.; Li, Z.; She, J.; Wang, W. Oxygen Density Dependent Band Gap of Reduced Graphene Oxide. *J. Appl. Phys.* **2012**, 111, 054317-054321.

(33) Shen, Y.; Yang, S.; Zhou, P.; Sun, Q.; Wang, P.; Wan, L.; Li, J.; Chen, L.; Wang, X.; Ding, S.; Zhang, D. W. Evolution of the Band-Gap and Optical Properties of Graphene Oxide with Controllable Reduction Level. *Carbon* **2013**, 62, 157-164.

(34) Rani P.; Jindal, V. Designing Band Gap of Graphene by B and N Dopant Atoms. *RSC Adv*. **2013**, 3, 802-812.